ISSN (e): 2250 – 3005 || Volume, 06 || Issue, 11|| November – 2016 ||
International Journal of Computational Engineering Research (IJCER)

Flow Control of Elastic Plates in Triangular Arrangement

Weishan Chen[1], Dibo Dong*, Zhenxiu Hou, Zhenbo Han
[1]State Key Laboratory of Robotics and System Harbin Institute of Technology Harbin, Heilongjiang Province, China

ABSTRACT

The hydrodynamicinteractions in fish schooling is a complex problem and still not well understood. In this work we use three flexible plates arranged in triangular as the model to study hydrodynamics interactions in fish schooling.The immersed boundary-lattice Boltzmann method (IB-LBM) is used to implement the simulation. By varying the interval distance and the expansion angle of the three plats, the drag, lift and flapping pattern of them are analyzed. The simulation results show that all the plates could flap passively in stable period in our simulation conditions. The dominated flapping frequencies of the three plates are always equal. The two downstream plates will flap synchronously and have the same amplitude in most cases. The upstream plate has a strong influence on the downstream two. We demonstrate four typical flapping patterns of the three plates at different interval distances and the expansion angles. When the plates are close to each other enough, the dynamics of them are like a single plate. Drag decrease can be obtained at certain distance. When the distance is big enough, the interactions between the three plates can be ignored, the dynamic of each plate is the same with that of the single plate. This work may offer inspiration for understanding the hydrodynamic interactions of fish schooling and the underwater robots designing.

Keywords: *flow control, flexible plate, passively flapping, fluid-structure interaction.*

I. Introduction

Fish schooling can promote the efficiency and benefit swimming [1]. The coupling of the fishes and flow environment is complex. The hydrodynamic interactions of fish schooling have been investigated by experiments and simulations. Flexible object like plate or filament is used as the model of fish body [2, 3] in previous researches. Two different interaction modes of double tandem flexible plates are observed in [4]: constructive mode and destructive mode, which will lead to an increase or decrease of drag on the downstream plate. Reference [5] investigates the flutter modes of two side-by-side flags. Six coupling modes of three parallel filaments are demonstrated in [6], the mode shift mainly depends on the distance between the filaments. The fish schooling has more complex arrangement than tandem or side-by-side, inspired by these two arrangements, three flexible plates arrange in triangular in a viscous flow is studied numerically in this paper. The hydrodynamic of the plates and flow in triangular arrangement should be more complicated compared with the tandem or side-by-side arrangement. The simulation is implemented by the immersed boundary-lattice Boltzmann method [7].

II. COMPUTATIONAL MODEL

Here we use three flexible plates as the model of fish bodies, a schematic diagram of three coupling flexible plates in triangular arrangement is shown in Fig. 1, the three plates is marked as P1, P2 and P3 as the figure shows. The three plate is immersed in a viscous flow with a uniform incoming velocity U_∞, which is parallel with the x-axis. All the lengths of the three plates are L. The leading edges of the plates are fixed and the trailing edges are in free motion. The leading edge of the P1 is placed at the center line of the fluid domain, the leading edges of the second and P3 are placed symmetrically about the center line. The interval distance D_p is defined as the distance between the leading edges of P1 and P3 along the x-axis. The dimensionless interval distance D is defined as $D = D_p / L$. The expansion angle θ is defined as the angle between the x-axis and the line which connecting the leading edges of P1 and P2.

The flow dynamics is governed by the Navier–Stokes and continuity equations:

$$\frac{\partial \boldsymbol{v}}{\partial t} + \boldsymbol{v}\cdot\nabla\boldsymbol{v} = -\nabla p + \frac{1}{Re}\nabla^2\boldsymbol{v} + \boldsymbol{f}_{ib} \tag{1}$$

$$\nabla \cdot \boldsymbol{v} = 0 \tag{2}$$

Where $\boldsymbol{v}$ is the velocity vector of the flow, t is the computational time defined as $t = L / U_\infty$, p denotes the pressure, $Re = \rho U_\infty L / \mu$ represents the Reynolds number.

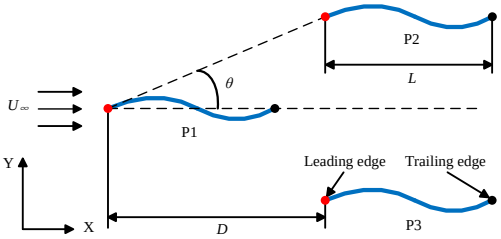

Fig.1 Schematic diagram of three coupling flexible plates in triangular arrangement.

μ is the dynamic viscosity of the flow, ρ is the flow density. $\boldsymbol{f}_{ib}$ is the interaction force added by the immersed boundary method. In IB-LBM, the fluid is divided into a regular Cartesian lattice and the fluid particles are on the nodes of the lattice, the moving plate is represented by a set of Lagrangian coordinate points. The lattice Boltzmann equation (LBE) [8] is used to simulate the dynamics of the flow instead of (1) and (2), which reads:

$$\frac{f_i(\mathbf{x} + \mathbf{e}_i \Delta t, t + \Delta t) - f_i(\mathbf{x}, t)}{(\Delta t)^2} = -\frac{f_i(\mathbf{x}, t) - f^{eq}(\mathbf{x}, t)}{\tau \Delta t} + \boldsymbol{F}_i \tag{3}$$

Where **x** is the coordinate of the flow's Cartesian lattice, f_i (**x**, t) is the distribution function for the flow particles at time t, position **x**. Δt is the time increment, τ is the relaxation time defined as $\tau = 3\mu + 0.5$. As shown in Fig. 2, $\mathbf{e}_i$ is the discrete velocity direction of the flow particles defined as:

$$\boldsymbol{e}_i = \begin{pmatrix} 0 & 1 & -1 & 0 & 0 & -1 & 1 & -1 & 0 \\ 0 & 0 & 0 & 1 & -1 & -1 & -1 & 1 & 0 \end{pmatrix} (i = 0, 1, \ldots, 8) \tag{4}$$

$f^{eq}(\mathbf{x}, t)$ is the equilibrium function which defined as:

$$f^{eq}(\mathbf{x}, t) = \rho \omega_i \left[1 + \frac{2\mathbf{e}_i \cdot \boldsymbol{v} - \boldsymbol{v}^2}{2c_s^2} + \frac{(\mathbf{e}_i \cdot \boldsymbol{v})^2}{2c_s^4} \right] \tag{5}$$

Where ω_i is the weight coefficient, c_s is the velocity of sound. $\mathbf{F}_i$ is the discretised force defined as:

$$\boldsymbol{F}_i = \omega_i \left(1 - \frac{1}{2\tau}\right) \left[\frac{\mathbf{e}_i - \boldsymbol{v}}{c_s^2} + \frac{\boldsymbol{v} \cdot \mathbf{e}_i^2}{c_s^4} \right] \cdot \boldsymbol{f}_{ib} \tag{6}$$

The flow density ρ and velocity $\boldsymbol{v}$ can are obtained by:

$$\rho = \sum_i f_i \,, \tag{7}$$

$$\rho \boldsymbol{v} = \sum_i \mathbf{e}_i f_i + \frac{1}{2} \Delta t \, \boldsymbol{f}_{ib} \tag{8}$$

The dynamics of the plate is governed by:

$$\rho_s \frac{\partial^2 \mathbf{X}}{\partial t^2} = \frac{\partial}{\partial s}\left(T \frac{\partial \mathbf{X}}{\partial s} \right) - K \frac{\partial^4 \mathbf{X}}{\partial s^4} - \boldsymbol{F}_{ib} = 0 \tag{9}$$

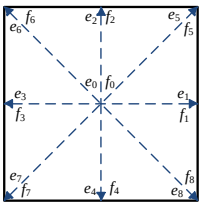

Fig. 2 Discrete velocity directions of the flow particles.

ρ_s is the plate's linear density. **X** is the coordinate of the plate's Lagrangian coordinate points, *s* denotes the parametric coordinate along the plate. $K = EI/(\rho U_\infty^2 L^3)$ is the bending stiffness, *EI* represents the plate's bending rigidity. $\boldsymbol{F}_{ib}$ denotes the force exerted by the plate's Lagrangian coordinate points on the flow particles. *T* is the tension inside the plate, which defined as

$$T = Eh\left(\left|\frac{\partial \mathbf{X}}{\partial s}\right| - 1\right) \tag{10}$$

Where *Eh* is the plate's stretching rigidity. As shown in Fig.3, (9) can be transformed into a staggered fashion by putting the tension points between each Lagrangian coordinate points:

$$\frac{\mathbf{X}^{n+1} - 2\mathbf{X}^n + \mathbf{X}^{n-1}}{\Delta t^2} = \frac{\left[D_s(T^{n+1} D_s \mathbf{X}^{n+1})\right] - K D_{ssss} \mathbf{X}^n - \boldsymbol{F}_{ib}^n}{\rho_s} \tag{11}$$

D_s is the standard second-order center finite difference with respect to *s*, *n* represents the number of the time steps. The flapping frequency of the plate's trailing edge is *f*. The flapping amplitude of the plate's trailing edge along the Y-axis is defined as A_p, the dimensionless flapping amplitude *A* is defined as $A = A_p / L$. The dimensionless mass ratio is defined as $M = \rho_s/(\rho L)$, the plate's drag coefficient and lift coefficient are $C_D = 2F_D/\rho U_\infty^2 L$ and $C_L = 2F_L/\rho U_\infty^2 L$, F_D and F_L denote the drag and lift force on the plate respectively.

The distances between each adjacent Lagrangian coordinate points and flow's Cartesian lattice nodes are set to 0.01. The plate' length is *L*, the flow domain is chosen as $40L \times 40L$. The lending edge of the P1 is fixed at (10*L*, 20*L*). The other governing parameters in all the simulations of this paper are: $Re = 100$, $M = 0.3$, $K = 10^{-4}$, $D = 1.0 - 3.0$, $\theta = 10^\circ - 60^\circ$. In such parameters, the plate's flapping motion can reach a stable state, the simulation results used for analysis are chosen from the stable periods.

III. RESULT AND DISCUSSION

Fig.4 shows the average C_D and the amplitude of C_L versus expansion angle θ at four different interval distance $D = 1.0$, 1.6, 2.2 and 3.0. The average C_D and the amplitude of C_L of P2 and P3 are always equal to each other, this result agrees with that of the two side-by-side plates [6]. At $D = 1.0$, the minimum C_D of the three plates occurs at $\theta = 10^\circ$, this is also the minimum interval distance between each of them, all the three plates experience a significant drag decrease compare with that of the single plate. Drag and lift of all the three plates increase with the expansion angle.

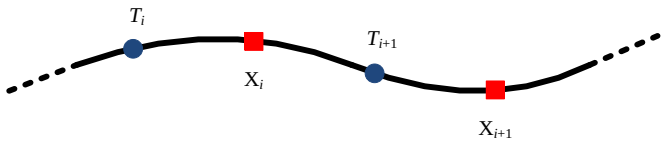

Fig. 3 Arrangement of the tension points and Lagrangian coordinate points on the plate.

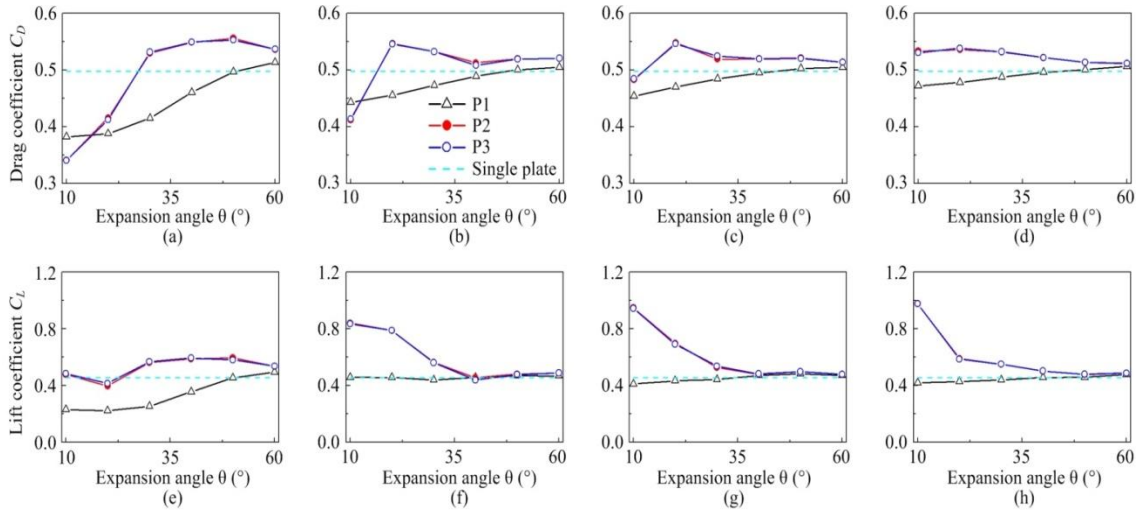

Fig. 4 The plates' average drag coefficient C_D and the amplitude of the lift coefficient C_L versus the expansion angle θ with (a), (e) $D = 1.0$, (b) (f) $D = 1.6$, (c) (g) $D = 2.2$, (d) (h) $D = 3.0$.

The drag and amplitude of lift is always smaller than that of P2 or P3, except at $\theta = 10^{\circ}$. At $\theta = 10^{\circ}$ - 40°, P1 experiences a drag reduction and the amplitude of lift decreases too.

For D = 1.6, 2.2 and 3.0, although drag on P1 is smaller compares with the single plate case, it is not so obvious as D = 1.0. With a larger D, the drag reduction is more unconspicuous. The amplitude of lift of P1 is almost equal to the single plate. Drag on P2 and P3 is larger than the single plate at most expansion angle and so is the amplitude of lift. At θ = 10°, the maximum C_L of P2 and P3 appears, then it decline sharply with the increase of the expansion angle. At θ = 40° - 50°, both the C_D and C_L of all the three plates approach to that of the single plate.

We can infer that when the interval distance D is small enough, P1 can enjoy a significant drag reduction. The downstream plates can work as a barrier [9], which can restrain the upstream plate's lateral flow, which lead to a drag reduction of the upstream plate. Smaller the distance is, the effect is more obvious, which conforms to the result shown in Fig. 4. Drag on P2 and P3 increase at the most cases because of the interactions of their upstream neighbor. When the distance between each plates is large enough, the interactions of them can be ignored, the C_D and C_L of them is almost equal to that of the single one.

Fig. 5 shows the plates' flapping amplitude A and flapping frequency f versus the expansion angle θ at D = 1.0, 1.6, 2.2 and 3.0. The flapping amplitude of P1 and P2 is almost equal. The three plates share the identical flapping frequency, so the frequency curves in Fig. 5 are represented by one plate. At D = 1.0, the flapping amplitude of P1 is obviously restrained at $\theta = 20^{\circ}$ - 40° and the amplitude of P2 and P3 are much larger. The minimum flapping frequency appears at $\theta = 10^{\circ}$, which also corresponds to the maximum amplitude. This is quite like the situation when two side-by-side plates are very close to each other.At D = 1.6, 2.2 and 3.0, the amplitude of P1 is always smaller than P2 and P3. At θ =10° - 30°, the amplitude of P2 and P3 is larger than the single plate case. With the increase of the expansion angle, the amplitudes of the three plates come close to the amplitude of single plate gradually. At θ =10° - 30°, the small flapping frequency always appears with large flapping amplitude. At θ =40° - 50°, both the amplitude and frequency of the three plate are very close to single plate.We can see from Fig. 5, the amplitude curves are similar with the lift coefficient curves. The amplitudes of P2 and P3 are always larger than that of P1 and single plate. The flapping frequency of the three plates is small when they are close to each other.

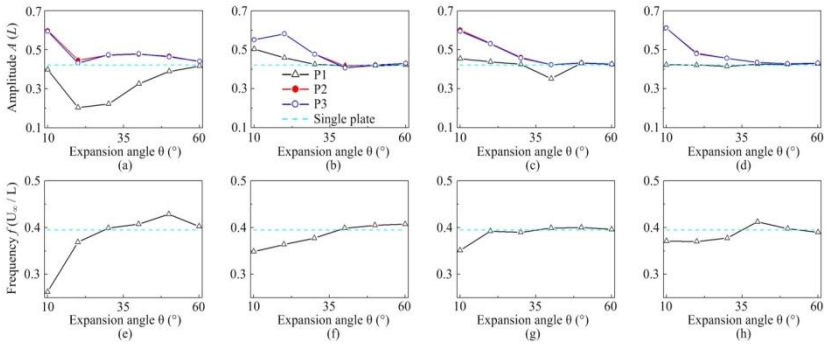

Fig.5 The plates' flapping amplitude A and flapping frequency f versus the expansion angle θ with (a), (e) D = 1.0, (b) (f) D = 1.6, (c) (g) D = 2.2, (d) (h) D = 3.0.

Based on the phase difference of the flapping motion and vorticity contours, we select several typical flapping patterns, as shown in Fig .6 to Fig .9.

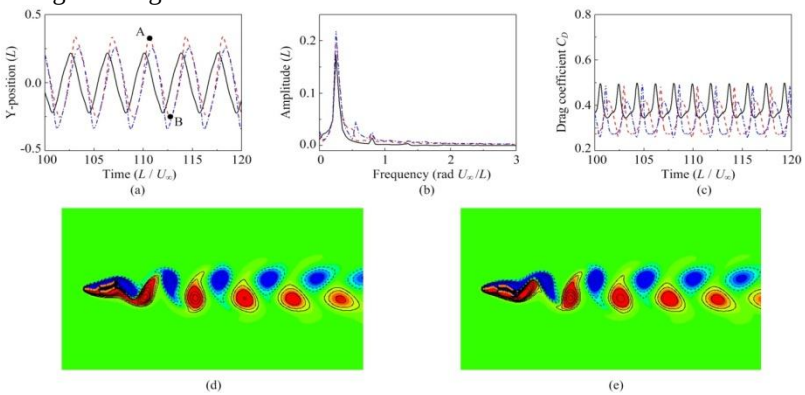

Fig. 6 Pattern I at D = 1.0, θ = 10° with (a) time history of plate's trailing edge Y-position, (b) FFT results of plate's flapping motion, (c) drag coefficient C_D (d) vorticity contours at time point A, (e) vorticity contours at time point B.

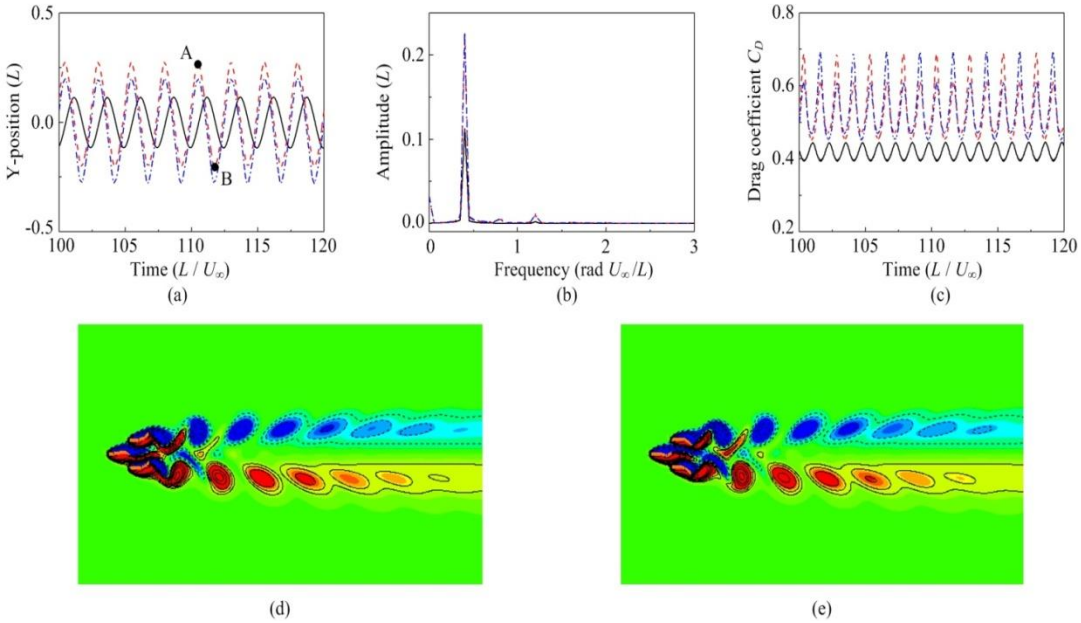

Fig. 7 Pattern II at D = 1.0, θ = 30° with (a) time history of plate's trailing edge Y-position, (b) FFT results of plate's flapping motion, (c) drag coefficient C_D (d) vorticity contours at time point A, (e) vorticity contours at time point B.

The first pattern at D = 1.0, θ = 10° is shown in Fig. 6. The three plates' interval distances in pattern I are smallest, in such small distance, the vortexes shedding by them merge together, which make the vorticity contours look like the these shedding by a single plate, the positive and negative vortexes arrange in a stagger form. In this pattern, the smallest drag is achieved. Because of the small distance, the flapping phase difference between P1 and P2 or P3 is not obvious. Pattern II at D = 1.0, θ = 30° is shown in Fig. 7. In this pattern, the flapping motion of P1 is restrained by the interactions of the two downstream plates, which leads to a significant drag reduction for P1. From the vorticity contours, we can see the vortexes shedding by P1 encounter with the opposite vortex generated by P2 and P3, which almost neutralizes the vortexes shedding by P1, the decrease of the vorticity leads to the small amplitude of P1. The collision of opposite vortexes also neutralizes the vortexes at the inner side of P2 and P3, as a result, only the vortexes at one side of P2 and P3 retained and move downstream with the flow as shown in Fig. 7 (d) and (e).

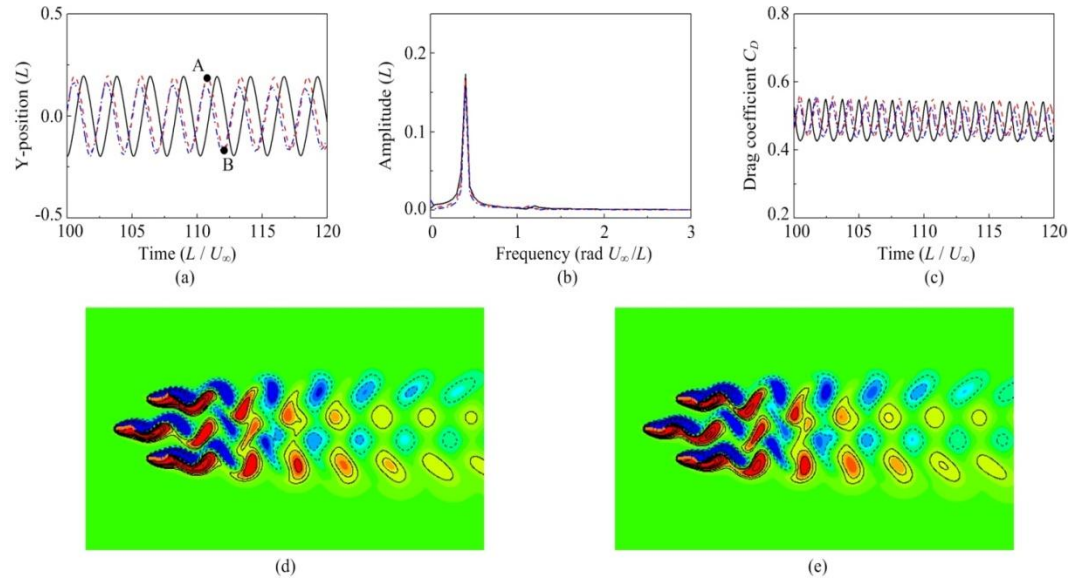

Fig. 8 Pattern III at D = 1.6, θ = 40° with (a) time history of plate's trailing edge Y-position, (b) FFT results of plate's flapping motion, (c) drag coefficient C_D (d) vorticity contours at time point A, (d) vorticity contours at time point B.

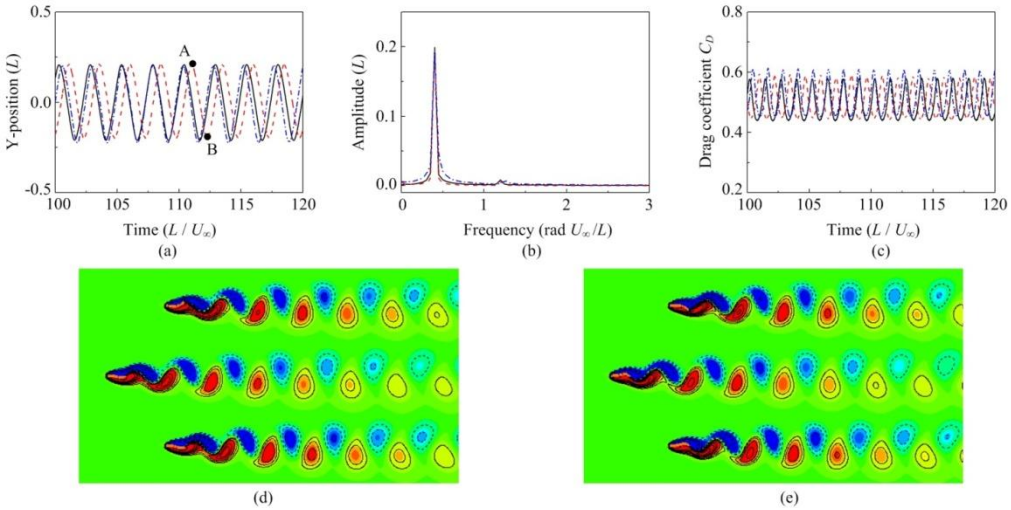

Fig. 9 Pattern IV at D = 3.0, θ = 50° with (a) time history of plate's trailing edge Y-position, (b) FFT results of plate's flapping motion, (c) drag coefficient C_D (d) vorticity contours at time point A, (d) vorticity contours at time point B.

Pattern III at D = 1.6, θ = 40° is shown in Fig. 8. Compared with the pattern I and II, the distances between each plates is larger and the interactions are not that obvious. All the three plates have similar flapping motions and the dynamics of them are close to the single plate. But the phase differences of Y-position of the tail and C_D still exist and the vortex of the three plates will merge at downstream, finally four lines of vortexes exist.
Pattern IV at D = 3.0, θ = 50° is shown in Fig. 9. In this pattern, the interval distances between each plates are big enough that the interactions can be almost ignored except the phase different still exist. The flapping motions of the two downstream plates in the former three patterns are all synchronous, but in pattern IV, there is a phase different between p2 and P3.We can see from the vorticity contours that the vortex shedding pattern by P1 have a strong influence on P2 and P3 in pattern I and II, which can induce their flapping motion to synchronize with the vortex they encountered. So the phase difference between P1 and P2 or P3 is decided by the interval distance D. This is like the case of two plates arranged in tandem.

IV. CONCLUSION

The hydrodynamic interactions of three flexible plates arrange in triangular in a viscous flow is studied numerically by IB-LBM. The dynamic characteristics of the plates are investigated by varying the interval distance D and expansion angle θ. We demonstrate four typical flapping patterns of the plates. For three plates arrange in triangular, the dominating flapping frequencies of them are always identical. In most cases the downstream two plates flap synchronously, the phase difference between the leading plate and the downstream ones is decided by the interval distance D. The minimum drag exists at the smallest interval distance and expansion angle, in this case the dynamics of them are similar with that of the single plate. With the increasing of the interval distance and expansion angle, the second pattern exists. The motion of the leading plate is restrained because of the interactions of the two downstream plates and drag on it obviously decreases. When the interval distance and expansion angle are big enough, the interactions of the three plates can be ignored, the hydrodynamic dynamics of each plate is the same with that of the single plate. The drag decrease can be achieved by placing the three plates in certain range of interval distance and expansion angle. This work could help understanding the dynamics of fish schooling and developing the underwater robots.

ACKNOWLEDGMENT

We would like to acknowledge sincerely the grant from National Natural Science Foundation of China (No. 50905040) and the Fundamental Research Funds for the Central Universities.

REFERENCES

[1] C. Hemelrijk, D. Reid, H. Hildenbrandt, and J. Padding. "The increased efficiency of fish swimming in a school," Fish and Fisheries, January 2014.
[2] W. Zhao, et al, "Theoretical and experimental investigations of the dynamics of cantilevered flexible plates subjected to axial flow," Journal of Sound and Vibration, vol. 331, no. 3, pp. 575-587, January 2012.
[3] H. Yuan, X. Niu, S. Shu, and M. Li, "A momentum exchange-based immersed boundary-lattice Boltzmann method for simulating a flexible filament in an incompressible flow," Computers & Mathematics with Applications, vol. 67, no.5, pp. 1039-1056, January 2014.

[4] S. Kim, W. Huang and H. Sung, "Constructive and destructive interaction modes between two tandem flexible flags in viscous flow," J. Fluid Mech, vol. 661, pp. 511–521, October 2010.
[5] S. Wang, W. Duan, and X. Yin, "Transition mode of two parallel flags in uniform flow," Chinese Physics Letters, vol. 30, no.11, p. 110502, May 2013.
[6] F. Tian, H. Luo, L. Zhu and X. Liu, "Coupling modes of three filaments in side-by-side arrangement," Physics of Fluids, vol. 23, no. 11, p. 111903, November 2011.
[7] J. Favier, A. Revell and A. Pinelli, "A Lattice Boltzmann–Immersed Boundary method to simulate the fluid interaction with moving and slender flexible objects," Journal of Computational Physics, vol. 261, pp. 145–161, March 2014.
[8] H. Yuan, X. Niu, S. Shu, and M. Li, "A momentum exchange-based immersed boundary-lattice Boltzmann method for simulating a flexible filament in an incompressible flow," Computers & Mathematics with Applications, vol. 67, no.5, pp. 1039-1056, January 2014.
[9] L. Ristroph and J. Zhang, "Anomalous hydrodynamic drafting of interacting flapping flags," Physical Review Letters, vol. 101, no. 19, p. 194502, November 2008.